

NMR relaxation in porous materials at zero and ultralow magnetic fields

Michael C. D. Tayler^{a,*}, Jordan Ward-Williams^a, Lynn F. Gladden^a

^aDepartment of Chemical Engineering and Biotechnology, University of Cambridge, Philippa Fawcett Drive, Cambridge, CB3 0AS, UK.

Abstract

NMR detection in the ultralow-field regime (below 10 μT) was used to measure the nuclear spin relaxation rates of liquids imbibed into silica pellets with mean pore diameters in the 10-50 nm range. Heptane, formic acid and acetic acid were studied and relaxation rate data were compared with a conventional field-cycling NMR technique. Detection of ^1H - ^{13}C spin coupling NMR signals at zero field (~ 0.1 nT) allowed spectroscopic identification of molecules inside the porous material and unambiguous measurements of the chemistry-specific relaxation rates in liquid mixtures. In the case of molecules that contain ^1H and ^{13}C , spin-singlet state relaxation can provide additional information about the dynamics. Applications and future improvements to the methodology are discussed.

Keywords: Nuclear magnetic resonance (NMR) relaxation, Fast field cycling, Zero-field NMR, Porous materials

1. Introduction

Porous materials – from rocks to heterogeneous catalysts – are extensively and widely studied. Of particular interest is to improve understanding of the behavior of fluids inside the pore structure; magnetic resonance techniques are uniquely positioned to address this because of their ability to probe inside the pore space[1, 2]. Magnetic resonance provides the opportunity to quantify molecular diffusion within the pore space using pulsed field gradient techniques[3, 4, 5, 6], while nuclear spin relaxation time measurements are now becoming established for characterizing the affinity of species for the pore surface. Relaxation rates are measured either at fixed field[7, 8, 9, 10] or at several values of applied magnetic field[11, 12, 13, 14, 15] to determine the spectral density function, and in turn the molecular dynamics, referenced to the NMR frequency.

Conventionally, a wide frequency range is studied via the fast-field-cycling (FFC) NMR method, where the pre-polarization, relaxation and detection stages of the measurement are performed at different magnetic fields, with rapid switching (< 5 ms) between field strengths[16, 17, 18]. FFC NMR instruments operate with switchable electromagnets over a proton (^1H) frequency range of tens of MHz (~ 1 T) to a few kHz (~ 200 μT) and can accurately quantify inter-molecular association and adsorption dynamics for correlation times up

to the order of 10 μs . A present limitation of FFC NMR is poor temporal field stability and homogeneity of the switchable magnets that make chemical-shift-resolved spectroscopy impossible. However, an inverse Laplace transform of the relaxation curve can separate environments where there are pronounced differences in rates, e.g. water and oil mixtures [19, 20]. An alternative approach, although not commonly applied to porous materials, is to shuttle the sample between different fields for relaxation and detection[21, 22, 23]. Subject to homogeneity of the applied field and magnetic susceptibility of the sample, one can profit from chemical shift resolution, but at the cost of a much longer field-switching time (> 100 ms) due to shuttling the sample.

In this paper, we report on nuclear spin relaxation in porous materials at much lower magnetic fields than those conventionally used in FFC NMR. Field strengths are from < 1 nT to a few mT, where the goal is to investigate aspects of surface-induced relaxation that hitherto have been inaccessible due to limited relaxation dispersion. The apparatus used is a sensitive alkali atomic magnetometer[24, 25, 26] inside a compact magnetic shield, which provides easy access to the field range below 100 μT , is scalable to the sample volume and is easy to operate. NMR detection at magnetic fields around 1 μT minimizes the effect of magnetic gradients on line width, resulting in a high single-scan signal-to-noise ratio. NMR detection at zero field, where nuclear spins have negligible Larmor frequency, allows specific chemicals to be resolved spectroscopically via

*Corresponding author

Email address: mcdt2@cam.ac.uk (Michael C. D. Tayler)

heteronuclear J couplings [27, 28, 29, 30, 31, 32]. The latter provides an opportunity to study nuclear relaxation in liquid mixtures.

2. Experimental methods

2.1. Materials and sample preparation

Relaxation rates were measured (a) for bulk liquids and (b) after imbibing the liquids into mesoporous silica pellets of varying pore size (FUJI Silysia CARIACT Q series, spherical pellets, 4 mm outer diameter). Mean pore size is denoted in nanometers as follows: Q-10 (10 nm mean pore diameter), Q-15 (15 nm), Q-30 (30 nm) and Q-50 (50 nm).

Bulk liquid samples: The following liquids were purchased from a chemicals supplier and degassed using several freeze-pump-thaw cycles before use: n-heptane ($\text{CH}_3(\text{CH}_2)_5\text{CH}_3$, 99%), [^{13}C]-formic acid (H^{13}COOH , 95 wt. % in H_2O , CAS: 1633-56-3) and [^{13}C]-acetic acid (> 99% $^{13}\text{CH}_3\text{COOH}$, glacial, CAS: 1563-80-0).

Approximately 0.15 mL of degassed liquid was pipetted into a 5.0 mm outer diameter (o. d.), 5 cm length borosilicate glass tube. The tube was purged with carbon dioxide and then flame sealed.

Porous silica samples: The spherical pellets were dried at 120 °C for 12 h before use. Four or five pellets were placed in a plastic Eppendorf vial then soaked in 0.2 mL of the degassed liquid for a further 12 h to saturation. Excess liquid was removed from the outside of the pellets before transfer into a 5 mm o. d. glass tube, which was then purged with carbon dioxide and flame sealed.

2.2. Ultralow-field NMR instrument

Ultralow-field NMR spectra and relaxation measurements were made in a magnetically shielded environment. A hot-vapor alkali magnetometer (^{87}Rb , 150 °C) with a sensitivity below 5×10^{-14} T/Hz $^{1/2}$ in the frequency range 0-400 Hz was used to detect the nuclear magnetization in DC bias magnetic fields up to a few μT .

As shown in Figure 1a, the magnetometer vapor cell and NMR sample are both placed in the center of four concentric cylindrical magnetic shielding cans (Twin-leaf LLC model MS-1F, mu-metal, outer shield diameter = 20 cm, length = 23 cm), where the magnetic background is below 10^{-10} T, setting a lower limit of magnetic field for the NMR experiment that is 4 to 5 orders of magnitude below the Earth's field. The magnetometer produces a voltage signal that is proportional to the total magnetic field along the z axis[33, 34]. Between

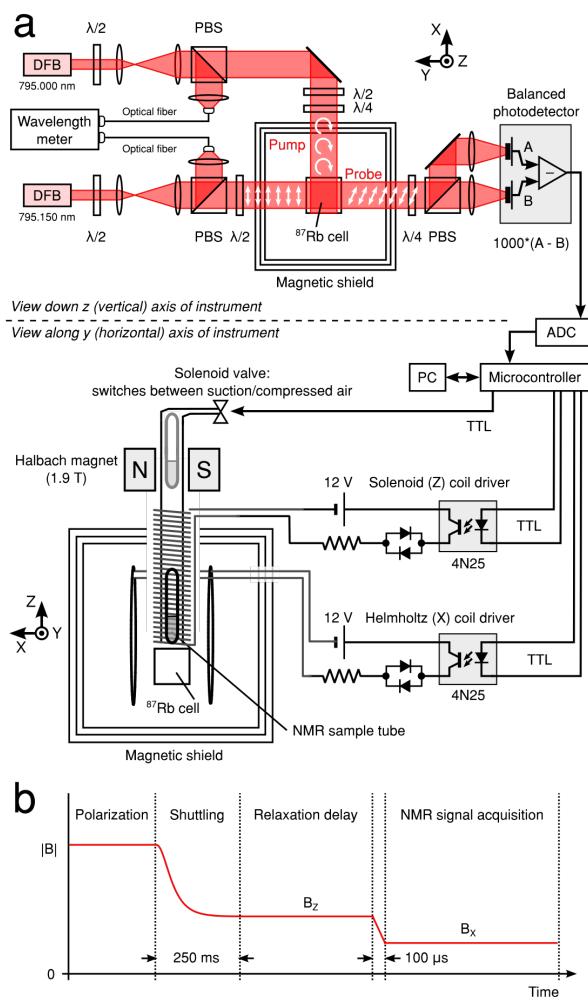


Figure 1: Field-cycling NMR instrument based on an optically pumped ^{87}Rb magnetometer: (a) the magnetic field due to ordered nuclear spins in the NMR sample is detected by magneto-optical rotation in a continuous-wave linearly polarized probing light beam near to the ^{87}Rb D1 transition ($5s^2S_{1/2} \rightarrow 5p^2P_{1/2}$, 795 nm). In the small-angle limit the difference of *s* and *p* polarized light intensities at the photodetector equals the optical rotation angle and produces a proportional output voltage. The NMR sample in a 5 mm outer-diameter glass tube is polarized in the Halbach magnet and then pneumatically shuttled inside the shield through a guiding solenoid (along z axis), which supplies the relaxation field. The Helmholtz coil (along x axis) provides a perpendicular DC magnetic field to drive nuclear Larmor precession after the solenoid coil is switched off. Field coils are switched on/off via an optocoupler and the field strength is varied by changing the current-limiting resistor; (b) Total magnetic field experienced by the sample during the NMR experiment. Abbreviations used: DFB = continuous-wave distributed-feedback laser diode; PBS = polarizing beam splitter; $\lambda/2$ = half-wave plate; $\lambda/4$ = quarter-wave plate; TTL = 5 volt transistor-transistor logic; ADC = analog-to-digital converter; PC = personal computer.

different bias fields the only necessary adjustment to the instrument is to zero the DC voltage output of the balanced photodetector. The signal is filtered (passband 1 Hz to 1 kHz), amplified (gain 1000) and then digitized with a low-cost microcontroller unit (Arduino UNO R3 [35] interfaced with a 16-bit analog-to-digital converter, sampling rate 4000 Hz). Data are then transferred to a laptop/personal computer via universal serial bus and stored in a file for processing later on. Further details of the magnetometer are given in ref. [26].

Relaxation measurements follow the timing sequence given in Figure 1b. A sample, sealed in a glass tube as described above, is polarized for 3 to 5 times the nuclear spin T_1 inside the bore of a Halbach magnet placed 10 cm vertically above the outermost shielding layer (field strength $B_{\text{pol}} = 1.9$ T, 7.5 mm magnet bore diameter, details given in ref. [36]). The sample is then pneumatically shuttled to the shield interior through a carbon-fiber tube (5.1 mm inner diameter, 7.3 mm outer diameter) passing through purpose-cut holes in the mu-metal. Typically, the sample shuttling takes 250–300 ms and the bottom of the tube comes to rest 2–3 mm above the hot alkali vapor cell. A thermocouple placed at the bottom of the shuttling tube shows the ambient temperature is in the range of 40–45 °C after equilibration in the air flow of the shuttling system (presently, active control of the sample temperature is not yet implemented). During the shuttling time a magnetic field is supplied along the z axis by a single-layer solenoid wound around the carbon-fiber tube (28 American wire gauge, 20 cm length, 5.8 mT/A). The field serves to adiabatically orient the nuclear magnetization along the z axis and also provide the relaxation field. Current up to 2 A can be supplied to the solenoid from a DC voltage source (12 V lead acid battery), an optical switch (4N25) and a shunt resistor, allowing the relaxation field to be switched up to ~ 3 mT. The maximum value of B_z is limited by the current rating of the circuit. Additional layers of coil windings can be added to increase the field 3–4 fold if desired, but are not employed in the present work.

A Helmholtz coil (230 $\mu\text{T/A}$, 20 mm radius, 6 loops of 28 American gauge wire on each side) was centered on the sample to supply a bias magnetic field along the x axis (B_x). After the relaxation delay time the solenoid (B_z) coil is rapidly switched off and the B_x coil is switched on. Nuclear magnetization then precesses in the yz plane at the Larmor frequency and the NMR signal is acquired (coil switching times < 20 μs). Data processing involves taking the Fourier transform of the time-domain magnetometer signal to extract the NMR signal amplitude. Repeating this process for a set of

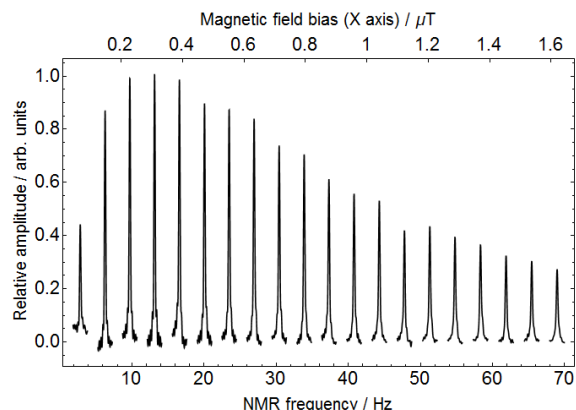


Figure 2: Variation in amplitude of ^1H Larmor precession NMR signal in distilled water (100 μL) due to dependence of magnetometer sensitivity on bias field and signal frequency. Displayed are the Fourier-transformed magnetometer signals between frequencies ($\nu_{\text{H}} - 2$ Hz) and ($\nu_{\text{H}} + 2$ Hz), where $\nu_{\text{H}} = \gamma_{\text{H}} B_x / (2\pi)$ is the ^1H Larmor frequency. Signal attenuation below 10 Hz is due to a high-pass filter between the photodetector and digitizer.

variable delays produces a curve of magnetization decay at the relaxation field B_z . Mono- or multi-exponential decay functions may be fitted to determine the relaxation rates. By repeating the process for different values of the shunt resistance, the rates can be measured as a function of B_z .

A value of $B_x = 0.7$ μT produced the highest ^1H free-precession signal amplitude against the magnetic noise background. Figure 2 shows relative signal amplitudes for ^1H free precession in a sample of 100 μL of distilled water versus the Larmor frequency up to $\nu_{\text{H}} = |\gamma_{\text{H}} B_x / 2\pi| = 68$ Hz ($B_x = 1.6$ μT , ^1H gyromagnetic ratio $\gamma_{\text{H}} = 42.576$ Hz/ μT). The signal amplitudes diminish with increasing $|B_x|$ according to a Lorentzian curve, which is due to the increased spin exchange relaxation in the alkali vapor[37]. However, signal-to-noise ratios are still in excess of 100 per scan around $B_x = 1$ μT , corresponding to a detection limit below 10 μL of the pure liquid. The half width at half maximum is approximately 0.08 Hz below 10 Hz frequencies and the increase over the field range indicates a homogeneity of ($|\Delta B_x / B_x| = (2100 \pm 150)$ ppm) across the sample.

2.3. Conventional fast-field-cycling relaxometry

Relaxation measurements were also made with a commercially produced field-cycling NMR instrument (Spinmaster 2000, Stellar Inc. [38]). A low-homogeneity unshielded electromagnet supplies relaxation fields between 250 μT and 1 T, and the NMR signal is detected at 0.39 T (16.3 MHz ^1H frequency). Field

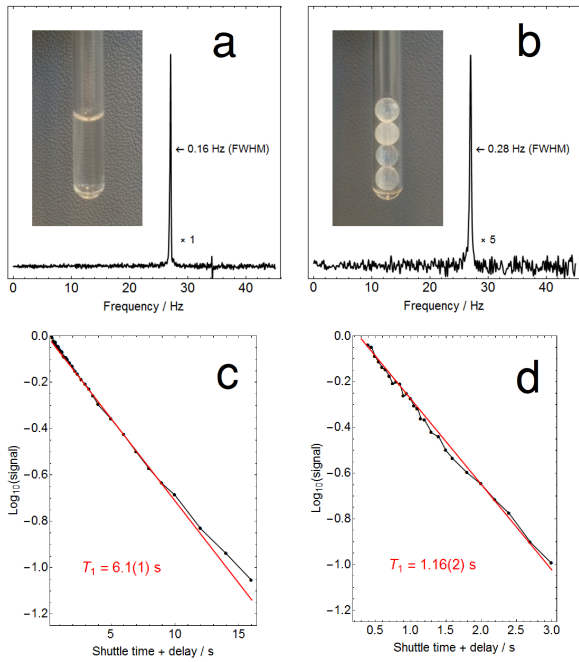


Figure 3: Single-scan NMR spectra and T_1 relaxation data recorded at $B_z = 0.634 \mu\text{T}$ (27 Hz ^1H Larmor frequency) for n-heptane in (a+c) bulk liquid and (b+d) imbibed into Q-15 porous silica.

switching times are 2-3 ms. In this unshielded configuration, the Earth's magnetic field is a large uncertainty in the total field strength and determines the lower limit for B_z . The sample temperature is regulated to within 1 °C by flowing heated air through the magnet bore.

Thus, the ultralow-field NMR and conventional fast-field-cycling relaxometry instruments provide concurrent measurements of relaxation – on the same NMR sample – over the field range $250 \mu\text{T} < B_z < 2.5 \text{ mT}$, i.e. one order of magnitude in field.

3. Results

3.1. Benchmarking of ultralow-field relaxometry with conventional approach

Longitudinal (T_1) relaxation measurements were made for samples of n-heptane (a) bulk liquid and (b) imbibed into Q-15 porous silica. The solvent was chosen because it does not react chemically or bind strongly with the surface of the porous silica. The expectation was a simple relaxation mechanism for a non-wetting liquid, which has been considered elsewhere[15].

The ^1H -precession NMR spectra shown in Figure 3(a+b) represent the typical line shapes and sensitivity. The spectra are presented in-phase and are the result of

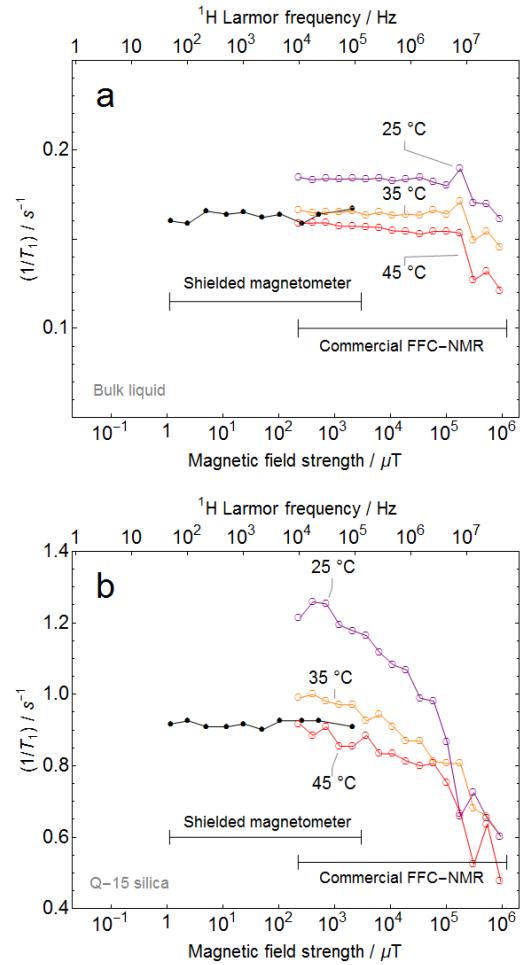


Figure 4: Dependence of ^1H longitudinal relaxation rate on B_z for n-heptane (a) bulk liquid and (b) imbibed into Q-15 silica.

a single acquisition (i.e. without averaging). The widths of the spectral lines at half height are 0.16 Hz (bulk) and 0.28 Hz (Q-15), corresponding to T_2^* values of 1.99 s and 1.14 s, respectively. The increase in ^1H NMR line width between bulk and Q-15 samples is due mainly to a reduction in the natural coherence lifetime (homogeneous broadening), and not the result of inhomogeneous broadening caused by the porous medium. For both samples a single scan provides a signal-to-noise ratio in excess of 30:1, and decay curves for ^1H longitudinal magnetization were measured without signal averaging. As an illustration, Figure 3(c+d) shows decay curves at a relaxation field of $B_z = 11 \mu\text{T}$, which are accurately fit by single exponential time constants: bulk liquid $T_1 = (6.1 \pm 0.1) \text{ s}$ and Q-15 silica $T_1 = (1.16 \pm 0.02) \text{ s}$.

Figure 4 shows the profile of $1/T_1$ versus B_z . For

the bulk liquid sample, both the commercial fast-field-cycling instrument and ultralow-field instrument show that the relaxation rate is independent of field below 1 mT, and that the curves overlap for a sample temperature of 40–45 °C. Small variations in the relaxation rate vs. field are the result of larger errors in the fitted relaxation times (caused by sample shuttling). These observations are consistent with the dominant relaxation process being caused by rapid fluctuations of the ^1H dipole-dipole coupling, which is modulated by translations and rotations on the picosecond timescale. The results suggest that the ultralow-field instrument provides a reliable extension of the relaxation curve down to Hz frequencies. For the Q–15 sample, consistent data are also obtained with the two instruments in the temperature range 40–45 °C. In this case the relaxation rate is strongly field dependent in the range 1 mT to 100 mT owing to transient adsorption of heptane molecules on the silica surface, but independent of field below ~ 1 mT. The observation of the “plateau” starting at 1 mT provides two key pieces of information. The first is that no additional relaxation mechanisms begin to contribute in the low-field/long-time limit and the second is the absolute value of the spectral density maximum. Both of these help the accurate fitting of models and elucidation of the underlying molecular dynamics of the system, but are not always accessible with conventional relaxometry. In other systems, the microtesla region of the relaxation curve may provide amplified contrast to differentiate between molecules in the system.

3.2. Chemically resolved NMR detection at zero field

NMR signals for different molecular species can be analyzed separately provided that their NMR frequencies are sufficiently dispersed. In high magnetic field, chemical shifts provide this dispersion. However, in the switchable magnets used for fast-field cycling, the magnetic field is not uniform enough to resolve chemical shifts at all. Even if the magnetic field were perfectly uniform, magnetic susceptibility gradient effects will degrade line widths by at least 0.5 ppm of the Larmor frequency, making it a challenge to resolve chemical shifts without resort to lengthy experiments involving insensitive nuclei (e.g. ^{13}C) or indirect detection (e.g. zero-quantum spectroscopy).

An alternative means of identification is to detect the NMR signal in the limit where the ambient magnetic field is below 1 nT (Larmor frequencies below 0.04 Hz), termed “zero field”. Directly observable NMR signals arise where nuclear polarization is exchanged between unlike spin species (e.g. ^{13}C plus ^1H) due to intramolecular scalar couplings and/or residual dipolar cou-

plings. A paragon of zero-field NMR in the liquid state is [^{13}C]-formic acid (H^{13}COOH). The alkyl proton and carbon are scalar coupled with $^1J_{\text{CH}} \approx 222$ Hz. If allowed to reach thermal equilibrium in a high magnetic field (B_{pol}) and then adiabatically shuttled into a weaker field oriented along the z axis (B_z), the state of the system is given by the following spin density operator

$$\begin{aligned} \rho = & 1/4 + [(\gamma_I + \gamma_S)(I_z + S_z) \\ & + (\gamma_I - \gamma_S)(I_z - S_z) \sin \theta \\ & + (\mathbf{I} \cdot \mathbf{S} - I_z S_z) \cos \theta] \hbar B_{\text{pol}} / 2k_B T, \end{aligned} \quad (1)$$

where spin operators represent $I = ^1\text{H}$, $S = ^{13}\text{C}$ and $\theta = \text{atan2}[(\gamma_I - \gamma_S)B_z, 2\pi J_{IS}]$; $J_{IS} = ^1J_{\text{CH}}$ (atan2 is the four-quadrant inverse tangent function). An observable NMR signal arises from the fact that while lines 1 and 3 of Equation 1 are stationary states at zero field, line 2 is not. Non-adiabatic switching of B_z to zero field ($|B| < 1$ nT) causes the $(I_z - S_z)$ component to oscillate at a frequency J_{IS} , producing an alternating magnetic field along the z axis that can be detected by the magnetometer. Similar results are found for small molecules that contain more than two spins; molecules with $A_N X$ spin topology (Pople notation: $I=A$ and $S=X$) yield zero-field NMR signals either at integer (odd N) or half-integer (even N) multiples of J_{IS} [30]. For instance, the $A_3 X$ system in [^{13}C]-acetic acid ($^{13}\text{CH}_3\text{COOH}$) will give signals at $1 \times ^1J_{\text{CH}} \approx 129$ Hz and $2 \times ^1J_{\text{CH}} \approx 258$ Hz.

Chemically resolved zero-field NMR detection provides a direct way to study low-field relaxation rates in mixtures and obtain insight into competition for adsorption at pore surfaces. The following liquids were studied in Q–50 and Q–15 porous silica: (i) [^{13}C]-formic acid, (ii) [^{13}C]-acetic acid and (iii) a binary liquid mixture made by combining the “stock” acids in a 1:1 volume ratio (to reach final concentrations of $\text{HCOOH} = 12.5$ mol dm^{-3} , $\text{CH}_3\text{COOH} = 8.4$ mol dm^{-3} and $\text{H}_2\text{O} = 3.2$ mol dm^{-3} before imbibing). The $^1J_{\text{CH}}$ NMR signals are displayed in Figure 5. Spectral line widths are inversely correlated with surface area to volume ratio, resulting in a less intense peak as the pore diameter decreases. However, the resonances remain clearly identified with the half-width at half maximum not exceeding 0.6 Hz.

These distinct spectral frequencies allow relaxation rates for each acid to be measured and fitted independently. In the limit $|\theta| \approx \pi/2$ the decay rate should approximate a mono-exponential decay where the time constant is close to the value of the proton T_1 . Measured rate data at $B_z = 130$ μT are plotted in Figure 6a.

The data show that formic acid has a higher relaxation rate in the binary liquid mixture than when absorbed

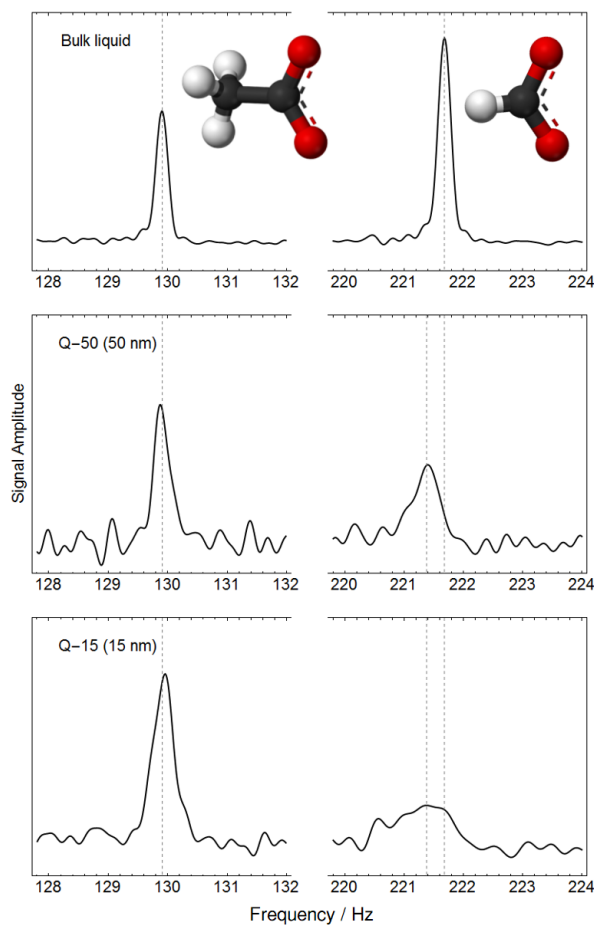


Figure 5: Zero-field NMR signals at the $^1J_{CH}$ resonance frequency for the mixture of $H^{13}COOH$ and $^{13}CH_3COOH$ in the bulk liquid and imbedded into Q-50 or Q-15 porous silica.

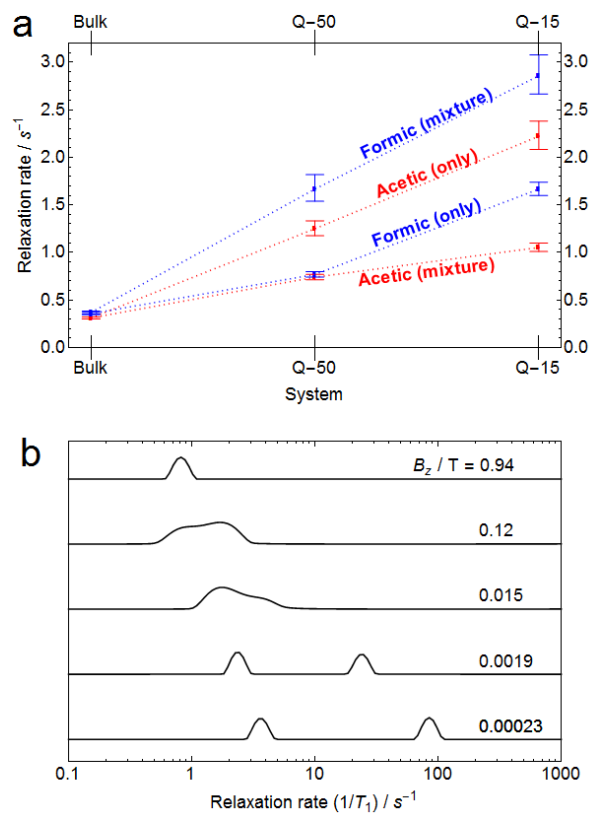


Figure 6: (a) Relaxation rates of $[^{13}C]$ -formic acid, $[2-^{13}C]$ -acetic acid and the 1:1 (ratio by volume) binary liquid mixture at $130 \mu T$. Dotted lines are used to guide the eye only; they are not “best fit” lines. (b) Relaxation curves for the liquid mixture in the Q-15 sample were measured on the commercial FFC-NMR instrument at logarithmic field strengths. The graph shows rate distributions obtained from the inverse Laplace transform of the data. The distributions were normalized to give a maximum peak height of 1.

as a single component. Conversely, acetic acid in the binary liquid mixture relaxes with a rate that is slower than as a single component. Qualitatively, these data are consistent with a relaxation model where molecules in the bulk of the pore space are rapidly exchanging with the surface (“two-site fast-exchange model”), hence the surface relaxivity is a time-weighted average of relaxation rates in the pore bulk and on the surface sites. In mixtures, the relaxivity of a molecule may increase or decrease relative to the single-component liquid depending on its affinity for the surface adsorption: for binary liquid mixtures, the relaxivity of the preferentially adsorbed component increases, while that of the other component decreases [7, 39]. The data here suggest that formic acid adsorbs more strongly than acetic acid.

The above conclusion cannot be reached with the commercial fast-field-cycling NMR instrument, where ^1H NMR line widths at the detection field (0.39 T) are the order of kHz and neither chemical shifts nor J couplings are resolved. Figure 6b shows the inverse Laplace transform of relaxation curves for the Q–15 silica imbibed with the binary liquid mixture. At low fields the inverse-Laplace “spectra” show two peaks corresponding to the acidic and alkyl ^1H environments. The indication is that the CHO and CH_3 relaxation rates cannot be differentiated, even though they differ by a factor of almost 3 according to the data in Figure 6(a).

3.3. Singlet state relaxation in H^{13}COOH

In the region near zero field ($|\theta| \ll 1$) the amplitude of $(I_z - S_z)$ produced by the shuttling method is too small to yield observable NMR signals. The NMR signal must be generated instead from the spin-singlet order $I \cdot S$ in Equation 1. This is achieved by applying a strong DC field ($B_{z,\text{pulse}}$) along the z axis (using the B_z solenoid coil) for a duration $\pi/[2(\gamma_I - \gamma_S)B_{z,\text{pulse}}]$ immediately before the data acquisition period [40]. During the preceding relaxation delay, singlet spin order decays with a different rate constant here denoted $1/T_S(I, S)$; the subscript denotes ‘singlet state’ and should not be confused with the spin species label S . Spin-singlet relaxation in H^{13}COOH and in other ^{13}C -containing liquids have been studied before at very low field, where it is observed that the intra-pair dipole-dipole mechanism does not contribute, while other dipole-dipole couplings only influence at very short-range distances[40, 41].

Field-dependent relaxation data recorded for H^{13}COOH in (a) bulk liquid, (b) Q–50 (c) Q–30 and (d) Q–10 silica are plotted in Figure 7a-d, respectively. Curves show mono-exponential relaxation rates that were fitted to the signal decay curves in the range

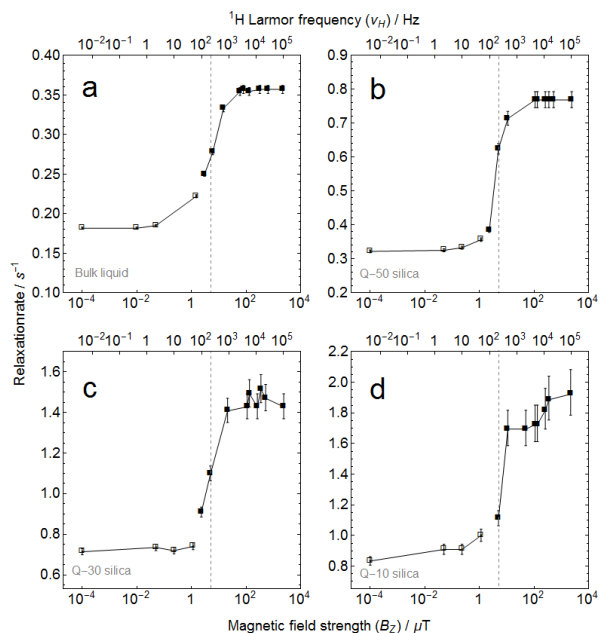


Figure 7: Field-dependence of relaxation rates for H^{13}COOH : (a) bulk liquid; imbibed into (b) Q–50, (c) Q–30 and (d) Q–10 silica. Plot markers denote whether the NMR signal is obtained from longitudinal polarization $I_z - S_z$ (■, rate tending to $1/T_1$ at mT field) or the singlet spin polarization $I \cdot S$ (□, tending to $1/T_S$ at zero field).

$0.1 \text{ nT} < B_z < 2.5 \text{ mT}$. The main observation is the occurrence of two plateau regions that define the limits of weak (where ^1H and ^{13}C relax individually with rates $1/T_1$) and strong coupling (tending to $1/T_S$ at zero field) – between which relaxation rates change by a factor close to 2. Filled square plot markers (■) indicate that the NMR signal was measured with the sequence of Figure 1b, while open square plot markers (□) indicate a DC excitation pulse was used.

The dashed vertical line shows the field for which $\tan \theta = 1$ (i.e. $[\gamma_I - \gamma_S]B_z = 2\pi J_{IS}$). The decay rate in this intermediate region is a smooth function of B_z (i.e. θ) due to strong mixing between $(I_z - S_z)$ and $I \cdot S$ in the eigenstates of the relaxation superoperator.

For bulk liquid H^{13}COOH a rate difference between zero-field $1/T_S$ and high-field $1/T_1$ is expected because the singlet order is not relaxed by the ^1H - ^{13}C dipole-dipole interaction. The value of 0.18 s^{-1} is reasonably accounted for by the rate contribution calculated from known C–H bond length and a molecular rotational correlation time of 12 ps. The non-zero rate $1/T_S$ is attributed to residual mechanisms, principally intermolecular dipole-dipole couplings and acidic ^1H exchange.

The data for H^{13}COOH in Q silica may be interpreted within a simple model where surface sites approximate

fluctuating random fields \mathbf{B}_I and \mathbf{B}_S at the nuclear sites and surface adsorption is represented with a single correlation time τ_c that is much faster than the NMR frequency. Predicted rate contributions are

$$1/T_1(I) = 2\tau_c\gamma_I^2 B_{I,\text{rms}}^2, \quad (2)$$

$$1/T_S(I, S) = 2\tau_c(\gamma_I^2 B_{I,\text{rms}}^2 + \gamma_S^2 B_{S,\text{rms}}^2 - 2c_{IS}\gamma_I\gamma_S B_{I,\text{rms}}B_{S,\text{rms}}), \quad (3)$$

where $B_{I/S,\text{rms}} = \langle \mathbf{B}_{I/S} \cdot \mathbf{B}_{I/S} \rangle^{1/2}$ are the root-mean-square amplitudes of the random field and $c_{IS} = \langle \mathbf{B}_I \cdot \mathbf{B}_S \rangle / (B_{I,\text{rms}}B_{S,\text{rms}})$ describes their instantaneous correlation. Assuming further that $B_{I,\text{rms}} = B_{S,\text{rms}}$, the ratio T_1/T_S depends only on c_{IS} . Experimental data are compared with this model by dividing the zero-field relaxation rate $1/T_S$ by the difference $1/T_1 - 1/T_S(\text{bulk})$, which produce values in the range of 0.5 to 0.6. These correspond to a correlation parameter c_{IS} above 0.95, implying near perfectly correlated fields $\mathbf{B}_{I/S}$.

If the relaxation mechanism proceeds via transient adsorption of molecules on surface sites, then the value of c_{IS} should depend strongly on the pore surface area to volume ratio. In the present case, there is no significant dependence observed. This may change for smaller pore diameters where there is a higher probability of molecular adsorption at surface sites. The relaxation mechanism is also undoubtedly more complicated than assumed in this model. For instance, the dynamics also involve chemical exchange with the aqueous/acid protons, which relax rapidly ($T_1 < 10$ ms). More detailed studies may be able to characterize the phenomenon and provide information about the nature of liquid-liquid and liquid-surface interactions, which cannot be readily obtainable elsewhere. This is a subject of ongoing work.

4. Discussion

The above experiments demonstrate ultralow-field NMR relaxation measurements on simple liquids confined in meso-porous silica. A sensitive atomic magnetometer enables liquids inside the porous matrix to be detected down to only a few tens of microliters in a single scan.

When operated in the most sensitive regime near zero field the magnetometer yields J-coupling spectra of molecules with a resolution given by the natural coherence line width, on the order of 0.1 to a few Hz. This allows independent fitting of relaxation rates for each chemical species regardless of the number of components in the system, provided that J couplings are resolved. In this case, the relative affinities of HCOOH

and CH₃COOH for the silica surface (Figure 6) were diagnosed from the relaxation rate of each acid when imbibed as a single liquid or part of a liquid mixture. Further studies may investigate surface competition involving additional species in the liquid, or the effect of surface treatments (e.g. modified wettability).

The zero-field NMR frequencies may provide information about the composition in the liquid in the porous material. The spectra in Figure 5 show a noticeable shift in the formic acid J coupling, $^1J_{\text{CH}}(\text{bulk}) - ^1J_{\text{CH}}(\text{Q-50}) = 0.3$ Hz. Quantitative measurements of composition in each sample via chemical-shift-resolved ¹H and ¹³C NMR at 9.4 T show that these shifts are most consistent with a preferential uptake of H₂O into the porous silica during imbibition, where the final concentration of water in the pellet appears to be 35 – 40% higher than that in the pre-imbibed liquid mixture.

The zero-field NMR spectra of H¹³COOH and ¹³CH₃COOH are relatively simple in appearance as there is only one value of ¹H-¹³C coupling in each molecule. Regarding application of the method to other molecules, one must consider that the complexity of the spin coupling topology and zero-field spectrum greatly increases with the number of magnetically inequivalent nuclei[30, 31]. Small molecules containing isolated groups of nuclei are therefore preferred. Acetyl (¹³CH₃CO-) and methoxy (¹³CH₃O-) chemical groups are immediate candidates for future studies to seek a further understanding of relaxation in the ¹³CH₃ group, which is also a subject of interest in hyperpolarized NMR and polarization storage [42, 43, 44]. Spin decoupling [45] or narrowband excitation pulse sequences [46] at zero field may also simplify the spectra and increase the scope for application to more complex molecules.

Finally, the avoidance of strong electromagnets in the ultralow-field instrument is an attractive feature, as the experimental setup consumes less than 100 W total electrical power and is compact enough to fit on a laboratory bench top. In future, we hope to modify the instrument to increase its potential for routine use:

(1) The magnetic field applied inside the shielded chamber by the electromagnetic coils can safely be increased to tens of mT without risk of saturating the mu-metal walls, which would allow one to measure relaxation dynamics in the MHz frequency range. These fields also present a realistic option for polarizing the sample when inside the shields. Such an approach would reduce the field switching times to only a few ms by eliminating the need to mechanically shuttle the sample. Presently, the sample shuttling prevents accurate measurements of relaxation rate above ~ 3 s⁻¹. A disad-

vantage of the suggested approach is a dramatic reduction in signal strength due to the lower polarization field (e.g. a 100× reduction between a 20 mT solenoid and a 2 T permanent magnet). However, the decay of polarization during field switching intervals is avoided and the magnetometer sensor can be scaled to larger detection volumes that compensate for the signal loss. Further improvements could be made by tuning the center frequency and bandwidth of the magnetometer to maximize sensitivity at the NMR frequency of interest[47].

(2) NMR relaxation rates depend strongly on the sample temperature, as seen in Figure 4. Concerning the proposed route of polarizing a stationary sample inside the magnetic shield, the temperature should be much easier to control and stabilize. To minimize thermal gradients and keep the sample close to room temperature, a cooling system or better insulation of the hot vapor cell may be needed. A cesium magnetometer may be a better choice as its lower vapor pressure allows similar sensitivity to be reached only slightly above room temperature [28, 48].

5. Conclusion

The experiments in this work demonstrate that NMR at zero and ultralow magnetic fields is a promising methodology to probe liquid-surface adsorption dynamics of molecules inside porous materials. A compact NMR instrument based on a rubidium magnetometer was used for relaxation measurements at mT down to nT fields, several orders of magnitude below Earth's field. In the limit of transient surface adsorption where induced relaxation is weak, NMR detection at zero field yields low-frequency dynamics information together with chemical resolution, which may be useful in quantifying composition and behavior of multi-component liquids in porous materials. The option of probing alternative relaxation pathways, including spin-singlet states, may allow further information about the interactions between solvent and surface to be obtained. In future, the technique may become applied to understand liquid-surface interactions in porous-solid-supported catalysts and rock cores.

Acknowledgment

The authors acknowledge Royal Dutch Shell plc. and the European Commission's Seventh Framework Program (grant agreement FP7-625054 ODMR-CHEM) for funding this work and thank Matthias Appel (Royal Dutch Shell plc.) for discussions. The author JWW acknowledges EPSRC for funding (grant EP/M507350/1).

References

- [1] J. H. Strange, L. Betteridge, M. J. D. Mallett, *Characterization of porous materials by NMR* in J. Fraissard, O. Lapina (eds) *Magnetic Resonance in Colloid and Interface Science*, NATO Science Series II, vol 76, pp 155-169 Springer, Dordrecht.
- [2] Y.-Q. Song, Magnetic resonance of porous media (MRPM): a perspective, *J. Magn. Reson.* 229 (2013), 12-24.
- [3] M. P. Hollewand and L. F. Gladden, Transport heterogeneity in porous pellets—II. NMR imaging studies under transient and steady-state conditions, *Chem. Eng. Sci.* 50 (1995), 309-326.
- [4] D. Weber, A. J. Sederman, M. D. Mantle, J. Mitchell and L. F. Gladden, Surface diffusion in porous catalysts, *Phys. Chem. Chem. Phys.* 12 (2012), 2619-2624.
- [5] J. Kärger and R. Valiullin, Mass Transfer in Mesoporous Materials: The Benefit of Microscopic Diffusion Measurement, *Chem. Soc. Rev.* 42 (2013), 4172-4197.
- [6] J. Kärger, Transport phenomena in nanoporous materials, *ChemPhysChem* 16 (2015), 24-51.
- [7] D. Weber, J. Mitchell, J. McGregor and L. F. Gladden, Comparing strengths of surface interactions for reactants and solvents in porous catalysts using two-dimensional NMR relaxation correlations, *J. Phys. Chem. C* 113 (2009), 6610-6615.
- [8] C. D'Agostino, G. L. Brett, P. J. Miedziak, D. W. Knight, G. J. Hutchings, L. F. Gladden and M. D. Mantle, Understanding the Solvent Effect on the Catalytic Oxidation of 1,4Butanediol in Methanol over Au/TiO₂ Catalyst: NMR Diffusion and Relaxation Studies, *Chem. Eur. J.* 18 (2012), 14426-14433.
- [9] J. Mitchell, T. C. Chandrasekera, D. J. Holland, L. F. Gladden and E. J. Fordham, Magnetic resonance imaging in laboratory petrophysical core analysis, *J. Phys. Rep.* 526 (2013), 165-225.
- [10] P. A. Vecino, Z. Huang, J. Mitchell, J. McGregor, H. Daly, C. Hardacre, J. M. Thomson and L. F. Gladden, Determining adsorbate configuration on alumina surfaces with ¹³C nuclear magnetic resonance time analysis, *Phys. Chem. Chem. Phys.* 32 (2015), 20830-20839.
- [11] S. Godefroy, J.-P. Korb, M. Fleury and R. G. Bryant, Surface nuclear magnetic relaxation and dynamics of water and oil in macroporous media, *Phys. Rev. E* 64 (2001), 021605.
- [12] S. Stapf and R. Kimmich, Molecular dynamics in confined monomolecular layers. A field-cycling nuclear magnetic resonance relaxometry study of liquids in porous glass, *J. Chem. Phys.* 103 (1995), 2247-2250.
- [13] J. Mitchell, L. M. Broche, T. C. Chandrasekera, D. J. Lurie, L. F. Gladden, Exploring surface interactions in catalysts using low-field nuclear magnetic resonance, *J. Phys. Chem. C* 117 (2013), 17699-17706.
- [14] J.-P. Korb., Nuclear magnetic relaxation of liquids in porous media, *New J. Phys.* 13 (2011), 035016.
- [15] J.-P. Korb., Multiscale nuclear magnetic relaxation dispersion of complex liquids in bulk and confinement, *Progr. NMR Spectrosc.* 104 (2018), 12-55.
- [16] F. Noack, NMR field-cycling spectroscopy: principles and applications *Progr. NMR Spectrosc.* 18 (1986), 171-276.
- [17] R. Kimmich, E. Ansaldo, Field-cycling NMR relaxometry, *Progr. NMR Spectrosc.* 44 (2004), 257-320.
- [18] R. M. Steele, J.-P. Korb, G. Ferrante, S. Bubic, New applications and perspectives of fast field cycling NMR relaxometry, *Magn. Reson. Chem.* 54 (2015), 502-509.
- [19] J. Ward-Williams, J.-P. Korb and L. F. Gladden, Insights into functionally specific adsorption dynamics and stable reaction intermediates using fast-field-cycling NMR, *J. Phys. Chem. C*, (2018), accepted.
- [20] J.-P. Korb, G. Freiman, B. Nicot, and P. Ligneul, Dynamical

- surface affinity of diphasic liquids as a probe of wettability of multimodal porous media, *Phys. Rev. E* 80 (2009), 061601.
- [21] A. G. Redfield, High-resolution NMR field-cycling device for full-range relaxation and structural studies of biopolymers on a shared commercial instrument, *J. Biomol. NMR* 52 (2012), 159-177.
- [22] Y. Gossuin, Z. Serhan, L. Sandiford, D. Henrard, T. Marquardsen, R.T.M. Rosales, D. Sakellariou, F. Ferrage, Sample shuttling relaxometry of contrast agents: NMRD profiles above 1 T with a single device, *Appl. Magn. Reson.* 47 (2016), 237-246.
- [23] S.F. Cousin, P. Kaderavek, B. Haddou, C. Charrier, T. Markad- sen, J.M. Tyburn, P.A. Bouvier, T. Speck, D. Vilhem, F. Engelke, W. Maas, D. Sakellariou, G. Bodenhausen, P. Pelu- pesty, F. Ferrage, High-resolution two-field nuclear magnetic resonance spectroscopy, *Phys. Chem. Chem. Phys.* 18 (2016), 33187-33194.
- [24] I. M. Savukov, Spin Exchange Relaxation Free (SERF) Magne- tometers. In: Grosz A., Haji-Sheikh M., Mukhopadhyay S. (eds) *Smart Sensors, Measurement and Instrumentation* book series, vol 19. (2016), pp 451-491 Springer.
- [25] P. J. Ganssle, H. D. Shin, S. J. Seltzer, V. S. Bajaj, M. P. Ledbet- ter, D. Budker, S. Knappe, J. Kitching, A. Pines, Ultra-low-field NMR relaxation and diffusion measurements using an optical magnetometer, *Angew. Chem. Intl. Edn.* 53 (2014), 97669770.
- [26] M. C. D. Tayler, T. Theis, T. F. Sjolander, J. W. Blanchard, A. Kentner, S. Pustelny, A. Pines and D. Budker, Instrumentation for nuclear magnetic resonance in zero and ultralow magnetic field. *Rev. Sci. Instrum.* 88 (2017), 091101.
- [27] J. W. Blanchard and D. Budker, Zero- to Ultralow-Field NMR, *eMagRes* (2016), 13951410.
- [28] Ledbetter, M. P., Crawford, C. W., Pines, A., Wemmer, D. E., Knappe, S., Kitching, J. and Budker, D., Optical detection of NMR J-spectra at zero magnetic field, *J. Magn. Reson.* 199 (2009), 25-29.
- [29] Ledbetter, M. P. and Budker, D., Zero-field nuclear magnetic resonance, *Physics Today*, 66 (2013), 44.
- [30] Butler, M., Ledbetter, M. P., Theis, T., Blanchard, J. W., Budker, D. and Pines, A., Multiplets at zero magnetic field: the geometry of zero-field NMR, *J. Chem. Phys.* 138 (2013), 184202-15.
- [31] Blanchard, J. W., Ledbetter, M. P., Theis, T., Butler, M., Budker, D. and Pines, A., High-resolution zero-field NMR J- spectroscopy of aromatic compounds, *J. Am. Chem. Soc.* 135 (2013), 3607-3612.
- [32] Theis, T., Blanchard, J. W., Butler, M., Ledbetter, M. P., Budker, D. and Pines, A., Chemical analysis using J-coupling multiplets in zero-field NMR, *Chem. Phys. Lett.*, 580 (2013), 160-165.
- [33] *Optical Magnetometry*, edited by D. Budker and D. F. Jack- son Kimball (Cambridge University Press (2013), ISBN: 1107010357.
- [34] I. M. Savukov, M. V. Romalis, NMR detection with an atomic magnetometer, *Phys. Rev. Lett.* 94 (2005), 123001.
- [35] <http://www.arduino.cc>
- [36] M. C. D. Tayler, D. Sakellariou, Low-cost pseudo-Halbach dipole magnets for NMR, *J. Magn. Reson.* 277 (2017), 143-148.
- [37] J. C. Allred, R. N. Lyman, T. W. Kornack, and M. V. Roma- lis, High-sensitivity atomic magnetometer unaffected by spin- exchange relaxation, *Phys. Rev. Lett.* 89 (2002), 130801.
- [38] G. Ferrante and S. Šykora, Technical aspects of fast field cy- cling, *Adv. Inorg. Chem.* 57 (2005), 405-470.
- [39] J. Ward-Williams and L. F. Gladden, Insights into adsorption behaviour of binary liquid mixtures in porous media using fast field cycling NMR, *Magn. Reson. Imag.*, (2018) accepted.
- [40] M. Emonds, M. P. Ledbetter, S. Pustelny, T. Theis, B. Patton, J. W. Blanchard, M. C. Butler, D. Budker and A. Pines, Long-lived heteronuclear spin-singlet states in liquids at a zero magnetic field, *Phys. Rev. Lett.* 112 (2014), 077601.
- [41] I. V. Zhukov, A. S. Kiryutin, A. V. Yurkovskaya, Y. A. Grishin, H.-M. Vieth and K. L. Ivanov, Field-cycling NMR experiments in ultra-wide magnetic field range: relaxation and coherent polarization transfer, *Phys. Chem. Chem. Phys.* 20 (2018), 12396-12405.
- [42] B. Meier, J.-N. Dumez, G. Stevanato, J. T. Hill-Cousins, S. S. Roy, P. Håkansson, S. Mamone, R. C. D. Brown, G. Pileio and M. H. Levitt, Long-lived states in methyl groups and quantum-rotor-induced polarization, *J. Am. Chem. Soc.* 135 (2013), 18746-18749.
- [43] J.-N. Dumez, P. Håkansson, S. Mamone, B. Meier, G. Stevanato, J. T. Hill-Cousins, S. S. Roy, R. C. D. Brown, G. Pileio and M. H. Levitt, Theory of long-lived nuclear spin states in methyl groups and quantum-rotor induced polarization, *J. Chem. Phys.* 142 (2015), 044506.
- [44] R. Annabestani and D. G. Cory, Dipolar relaxation mechanism of long-lived states of methyl groups, *Quantum Inf. Process.* 17:15 (2018), Springer.
- [45] T. F. Sjolander, M. C. D. Tayler, A. Kentner, D. Budker and A. Pines, ¹³C-decoupled J-coupling spectroscopy using two- dimensional nuclear magnetic resonance at zero field, *J. Phys. Chem. Lett.* 8 (2017), 1512-1518.
- [46] T. F. Sjolander, M. C. D. Tayler, J. P. King, D. Budker and A. Pines, Transition-selective pulses in zero-field nuclear magnetic resonance, *J. Phys. Chem. A* 120 (2016), 4343-4348.
- [47] I. M. Savukov, S. J. Seltzer, M. V. Romalis, Detection of NMR signals with a radio-frequency atomic magnetometer, *J. Magn. Reson.* 185 (2007), 214-220.
- [48] Liu, G., Li, X., Sun, X., Feng, J. Chaohui, Y., and Zhou, X., Ultralow field NMR spectroscopy with an atomic magnetometer near room temperature, *J. Magn. Reson.* 237 (2013), 158-163.